

Table S1: Steered Molecular Dynamics Parameters

Parameter	Setting
Time step	2fs
Number of steps (Time) for 1nm/ns	10000000 (20ns)
Number of steps (Time) for 10nm/ns	1500000 (3ns)
Integrator	Leapfrog algorithm
Constraint Algorithm	LINEar Constraint Solver (LINCS)
Constraints	H-bonds constrained
Cutoff scheme	Verlet (Buffered neighbor searching)
Short-range neighbor list cutoff	1.4nm
Short-range electrostatic cutoff	1.4nm
Short-range van der Waals cutoff	1.4nm
Electrostatics	Fast smooth Particle-Mesh Ewald (SPME)
Interpolation order	Cubic
Grid spacing for fast Fourier Transform	0.12nm
Temperature coupling	Nosé-Hoover
Reference temperature	310K
Temperature time constant	1.0ps
Temperature coupled groups	Protein and non-protein
Pressure coupling	Off
Dispersion correction	long range dispersion corrections for energy and pressure
Velocity generation	Off
Harmonic potential	Umbrella
Force constant	50 kJ/mol-nm ²
Pull direction	y-direction (vertical)
Pull rate for 1nm/ns	0.001nm/ps = 1nm/ns
Pull rate for 10nm/ns	0.010nm/ps = 10nm/ns

Table S2: Time resolved Force Distribution Analysis Parameter Settings

Parameter	Setting
Pairwise forces	Summed
Pairwise groups	Protein
Residue based calculation	Punctual Stress
Pairwise force type	Coulombic interactions only

Table S3: Catch bond parameters for whole-cell finite element model

Variable	Wildtype	R1374/9A
K_{on}	0.1 s^{-1}	0.02 s^{-1}
K_a	0.4 s^{-1}	0.8 s^{-1}
K_b	$4E - 7\text{s}^{-1}$	$8E - 7\text{s}^{-1}$
F_a		-25pN
F_b		-15pN

Table S4: Measured extension rate (nm/ns) of $\alpha_5\beta_1$ -FN under load in reference to the (i) peak and (ii) valley force as seen in Figure 2A-D

	Prior to (i)	Between (i) and (ii)	After (ii)
10nm/ns wildtype	5.10	14.4	9.21
10nm/ns R1374/9A	4.17	13.2	9.15
1nm/ns wildtype	0.547	1.82	0.546
1nm/ns R1374/9A	0.705	1.63	0.562

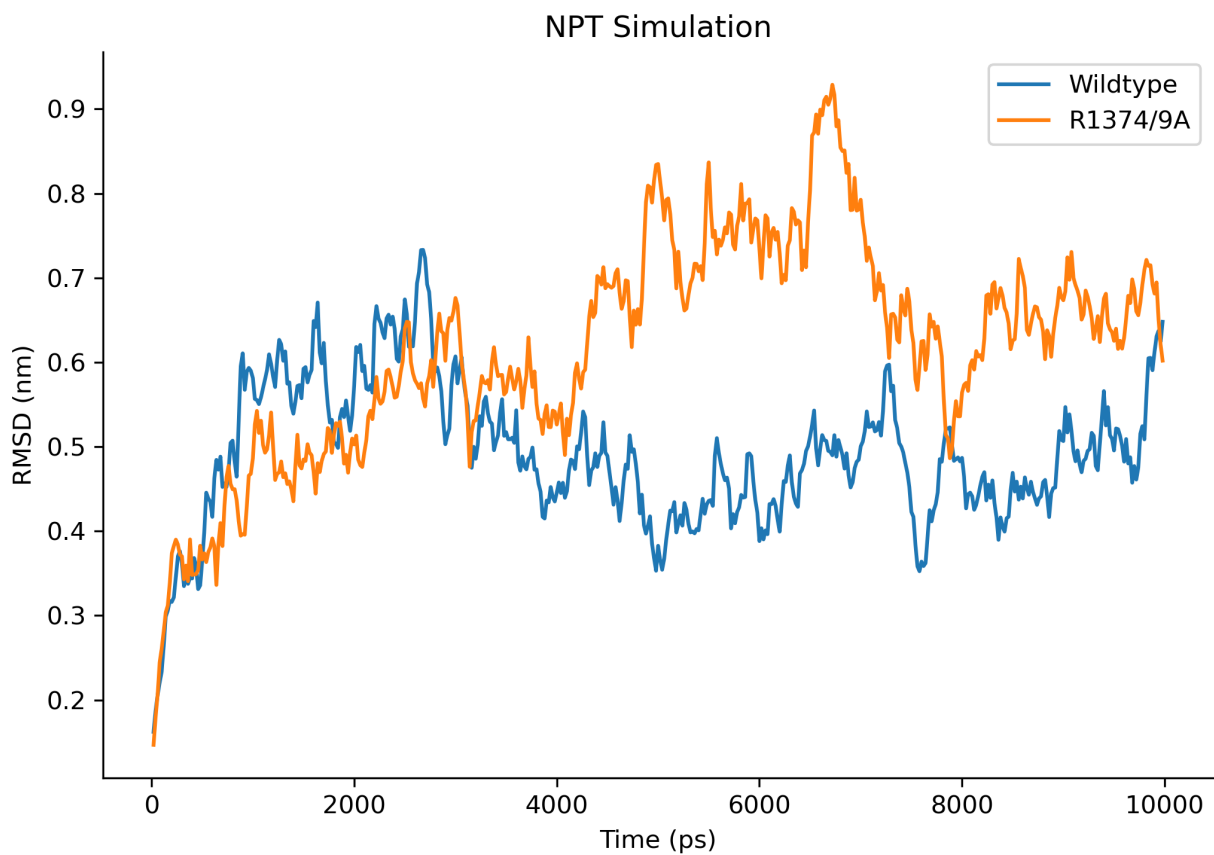


Figure S1: Root-mean-square deviation (RMSD) of wildtype and mutant during NPT simulation

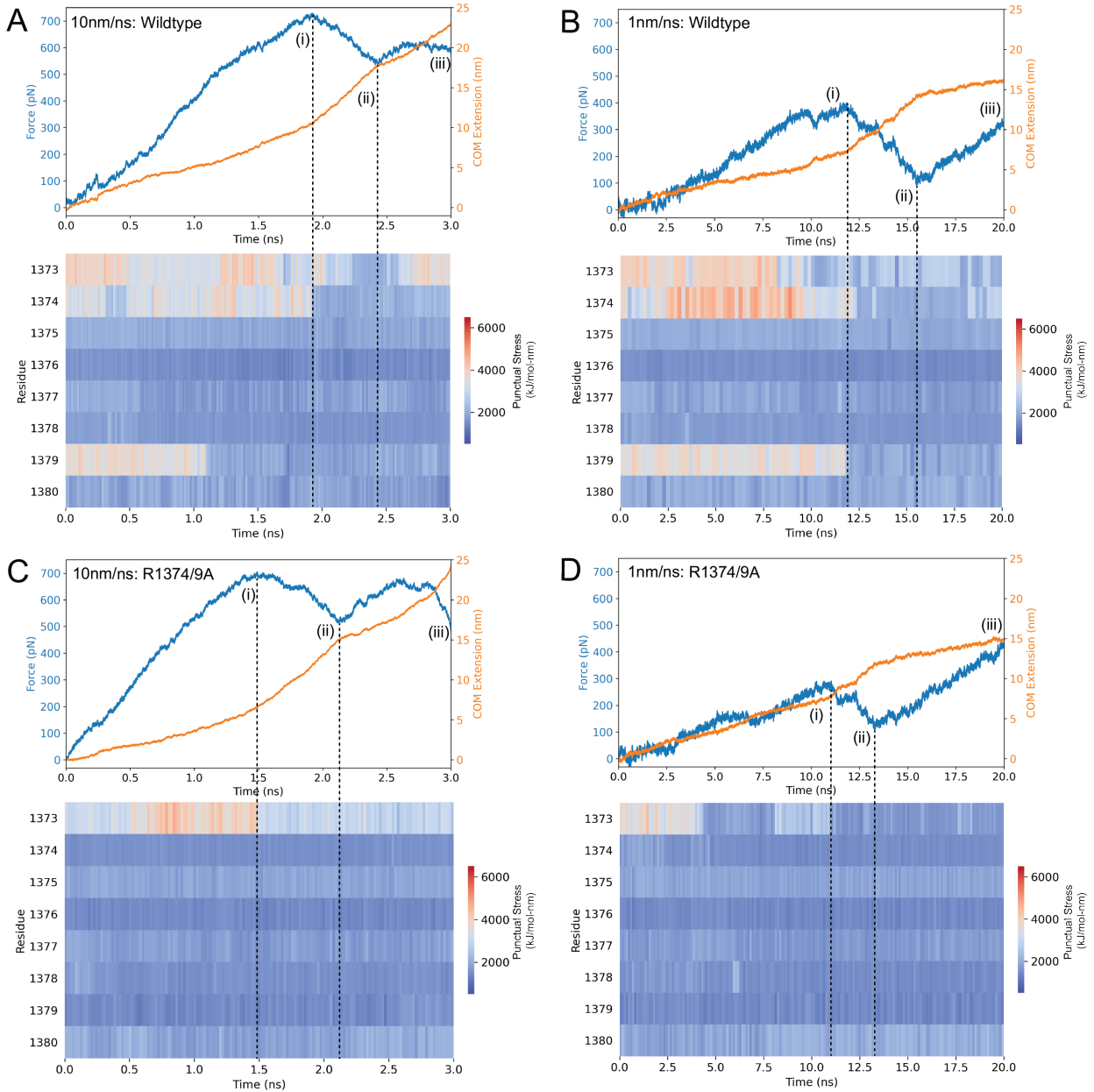


Figure S2: Force and COM extension over time plotted over punctual stress at the synergy site [1373-1380] for A) 10nm/ns wildtype $\alpha_5\beta_1$ -FN, B) 1nm/ns wildtype $\alpha_5\beta_1$ -FN, C) 10nm/ns R1374/9A $\alpha_5\beta_1$ -FN, and D) 1nm/ns R1374/9A $\alpha_5\beta_1$ -FN. Positions (i), (ii), and (iii) correspond to the time at the peak force, local minimum, and final frame, respectively.

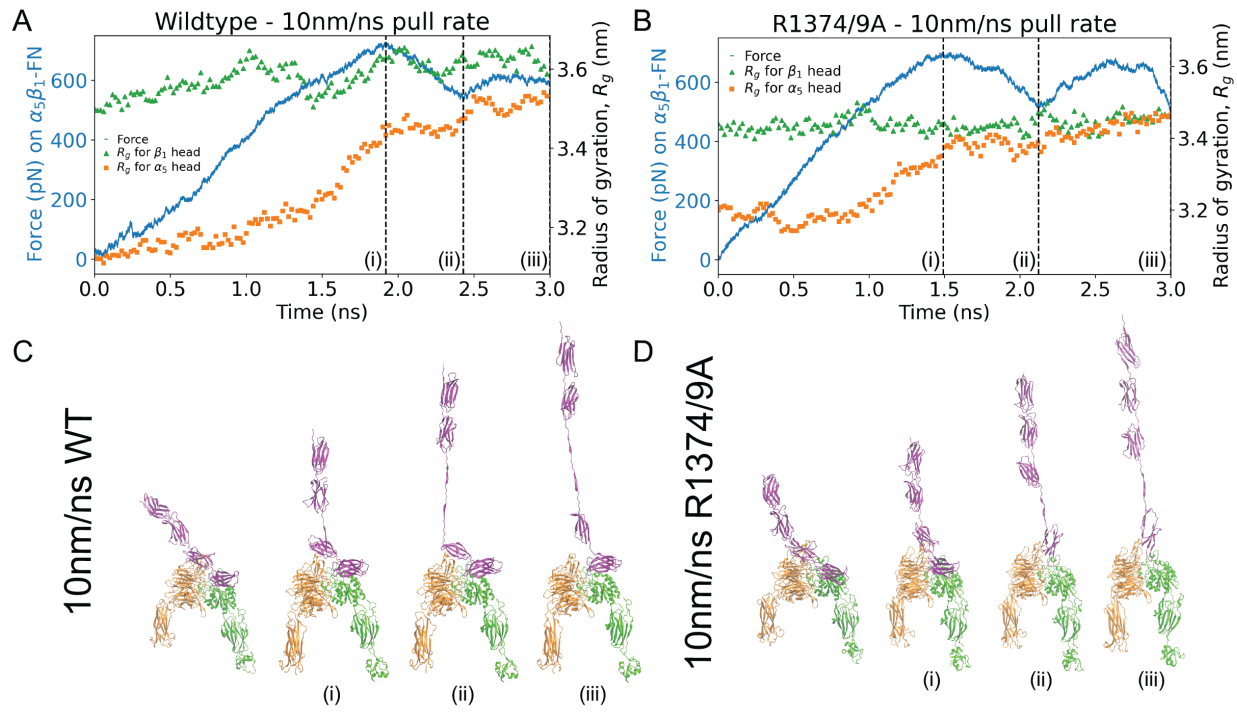


Figure S3: Force on $\alpha_5\beta_1$ -FN and radius of gyration of α_5 and β_1 head for the 10nm/ns runs for the A) wildtype and B) mutant. Positions (i), (ii), and (iii) correspond to the time at the peak force, local minimum, and final frame. The four shown frames from the simulation correspond to the first frame, (i) peak force, (ii) local minimum, and (iii) final frame for C) wildtype and D) mutant.

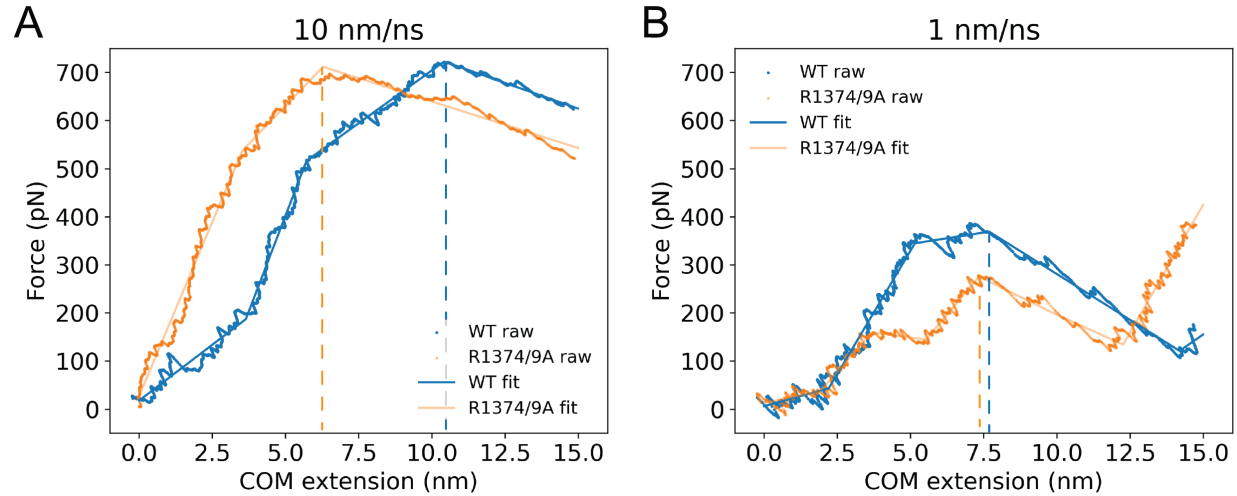


Figure S4: Force-extension plots for A) 10nm/ns and B) 1nm/ns pull rates. Dashed lines indicate the extension at the synergy site departure force. A moving average with a window size of 10ps was applied to the raw data for visualization purposes only. The piece-wise linear fit was performed over all points.

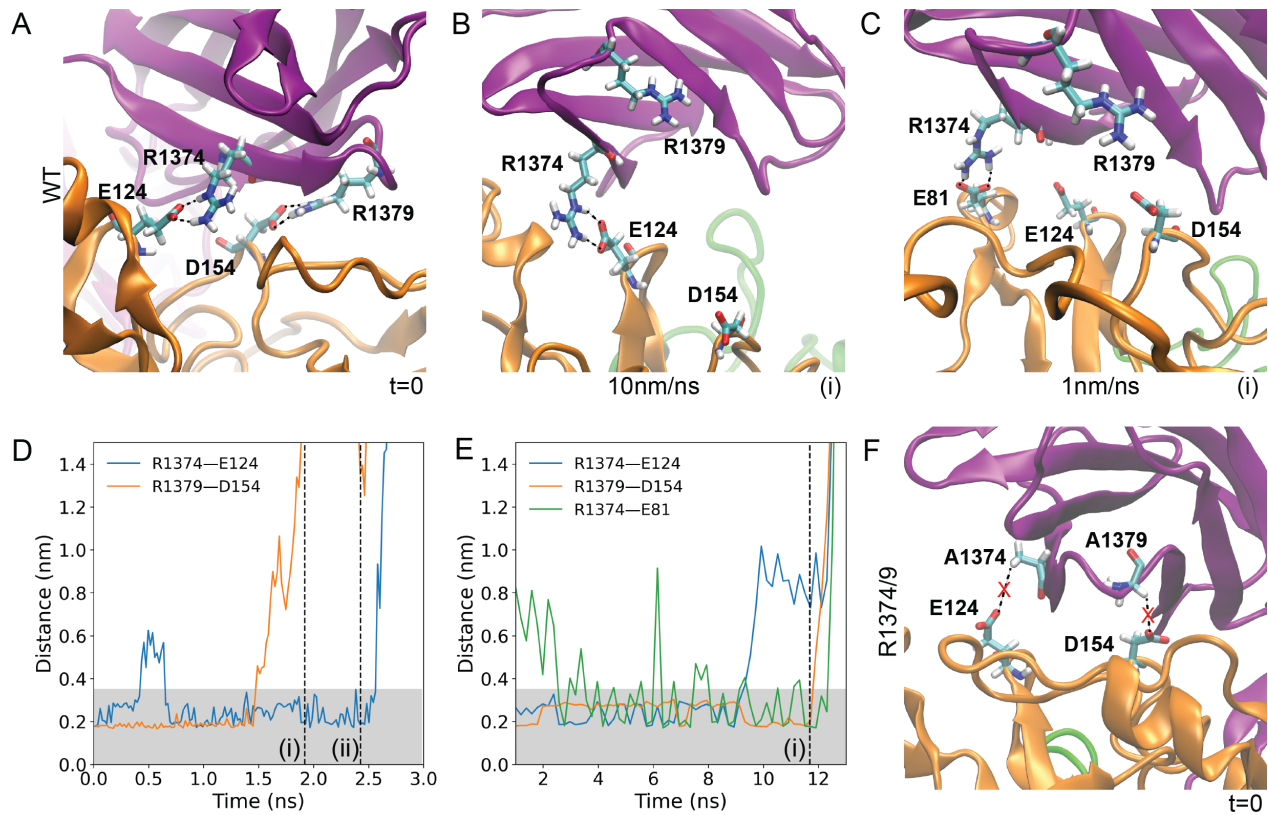


Figure S5: A) Interactions between R1374—E124 and R1379—D154 at the beginning of the wildtype simulations. B) At the force peak of the 10nm/ns wildtype simulation, the R1379—D154 salt bridge was broken but R1374—E124 remained. C) At the force peak of the 1nm/ns wildtype simulation, the R1379—D154 salt bridge was broken and R1374 formed a new hydrogen bond with E81. D) Distance between R1374—E124 and R1379—D154 for the 10nm/ns wildtype simulation. E) Distance between R1374—E124, R1379—D154, and R1374—E81. Shaded regions indicate 0.35nm, or the assumed approximate length for a hydrogen bond. The vertical dashed line is the time point of the force peak. F) The R1374/9A double mutation separated the A1374—E124 and A1379—D154 bonds to over 0.65nm, preventing hydrogen bond formation.

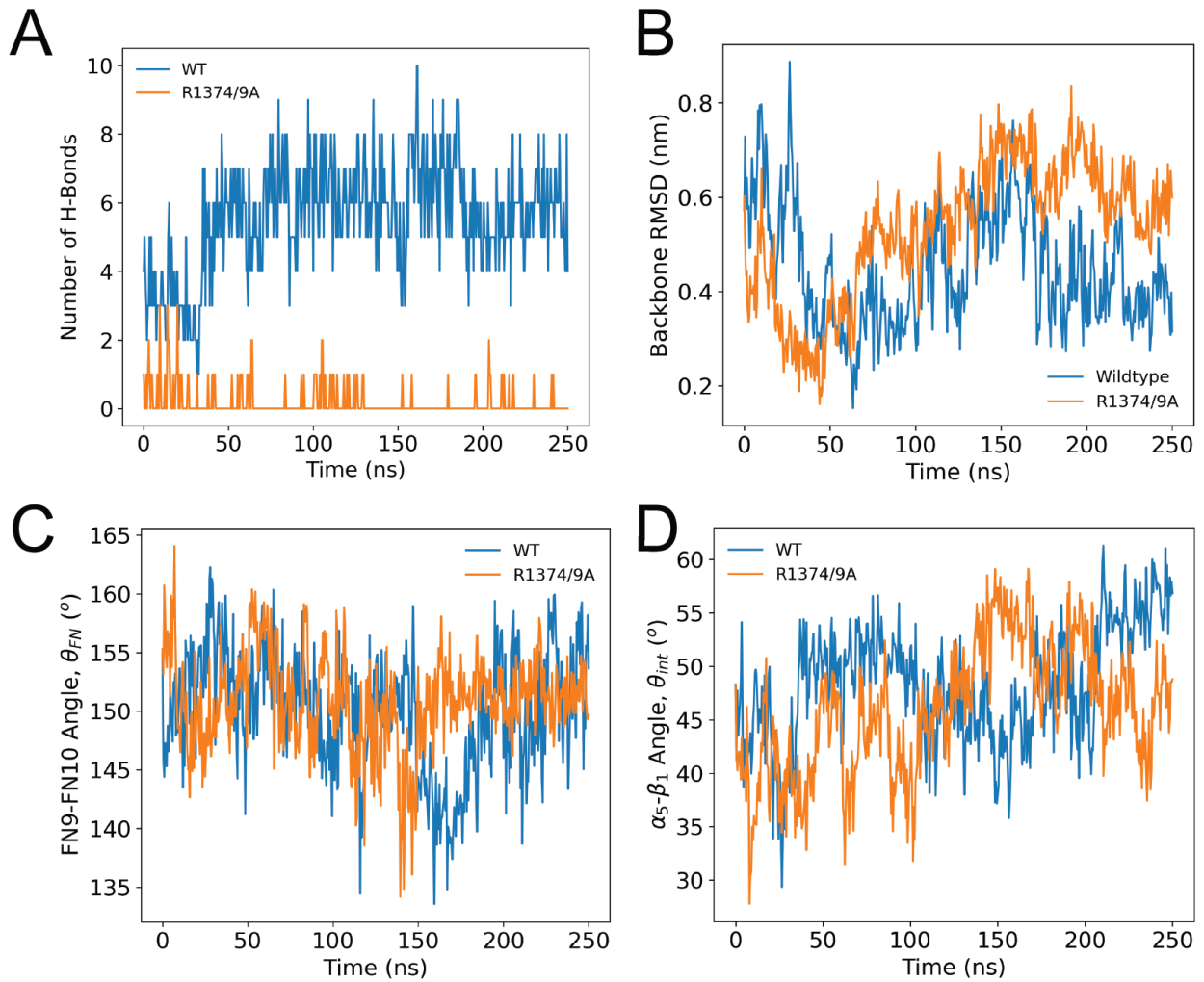


Figure S6: A) Number of hydrogen bonds, B) Backbone RMSD, C) FN9-FN10 Angle, and D) $\alpha\text{-}\beta_1$ angle over the 250ns simulation of the wildtype (WT) and mutant.

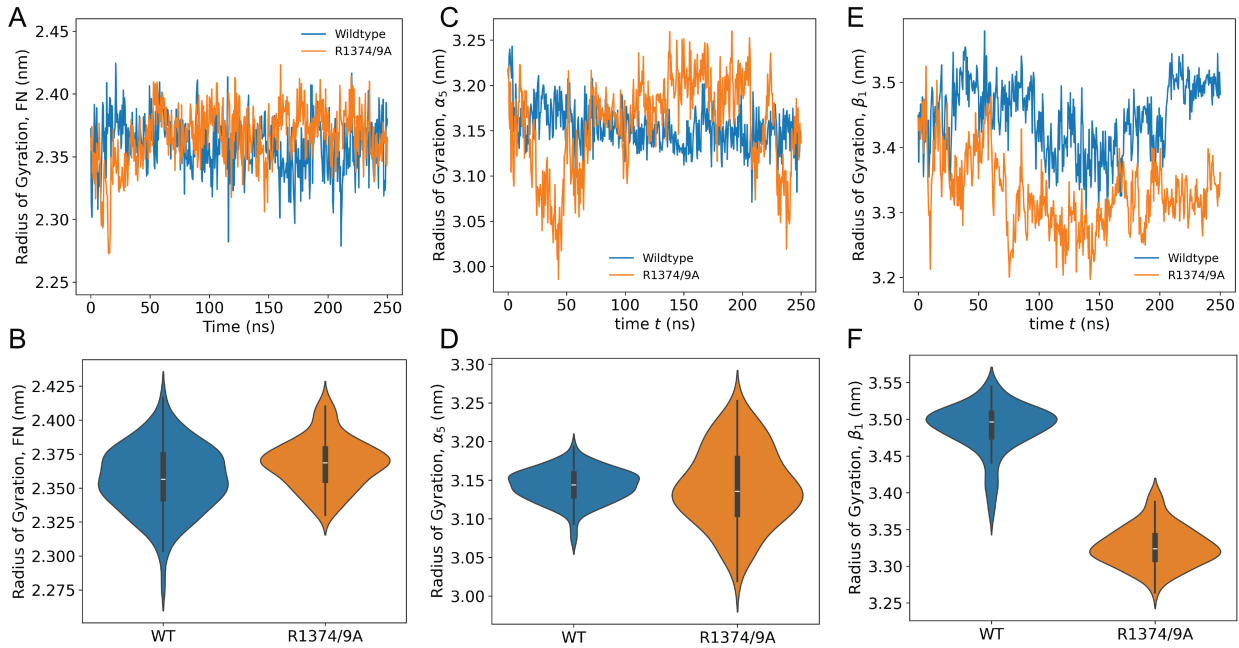


Figure S7: Time series data and violin plots of the radius of gyration of A-B) FN9-10 (WT = 2.36 ± 0.02 nm, R1374/9A = 2.37 ± 0.02 nm, $p = 0.0004$), C-D) the α_5 head (WT = 3.14 ± 0.02 nm, R1374/9A = 3.14 ± 0.05 nm, $p = 0.73$), and E-F) the β_1 head (WT = 3.49 ± 0.03 nm, R1374/9A = 3.33 ± 0.03 nm, $p < 0.00001$)

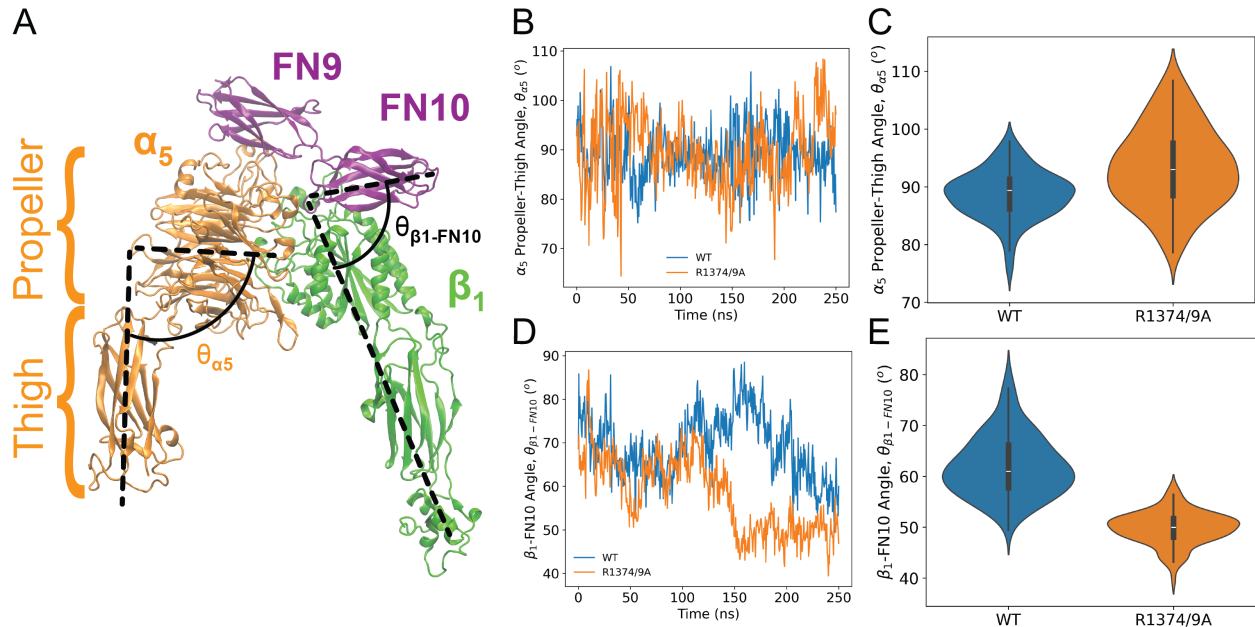


Figure S8: A) Cryo-EM structure of $\alpha_5\beta_1$ -FN9-10 with the thigh propeller angle ($\theta_{\alpha 5}$) and the β_1 -FN10 angle (θ_{β_1-FN10}) labeled. B) Time series data of $\theta_{\alpha 5}$. C) Violin plots of $\theta_{\alpha 5}$ (WT = $88.7 \pm 4.2^\circ$, R1374/9A = $93.4 \pm 6.8^\circ$, $p = 0.3$). D) Time series data of θ_{β_1-FN10} . E) Violin plots of θ_{β_1-FN10} (WT = $62.0 \pm 6.0^\circ$, R1374/9A = $49.9 \pm 3.2^\circ$, $p < 0.00001$).

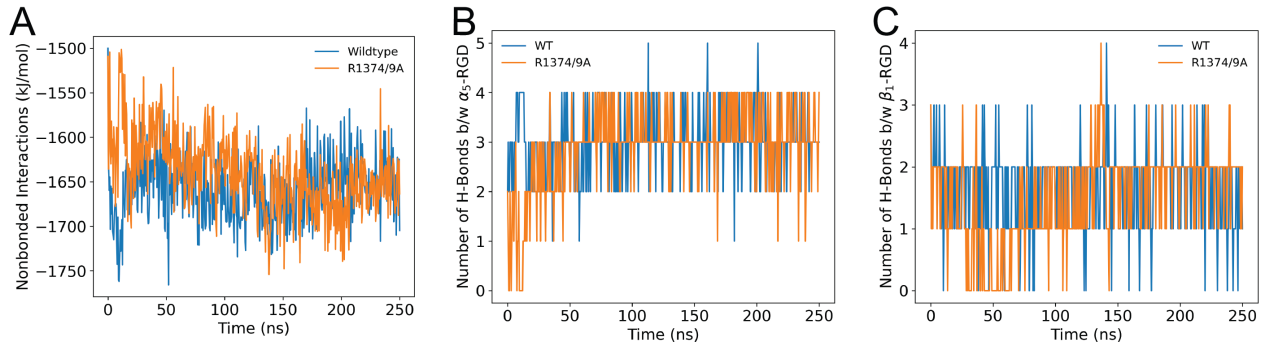


Figure S9: A) Nonbonded interactions at the RGD site which is the summation of the coulombic and van der waals energies for α_5 -MIDAS, α_5 -RGD, β_1 -MIDAS, β_1 -RGD, and RGD-MIDAS. B) Number of H-bonds between α_5 and RGD. C) Number of H-bonds between β_1 and RGD.

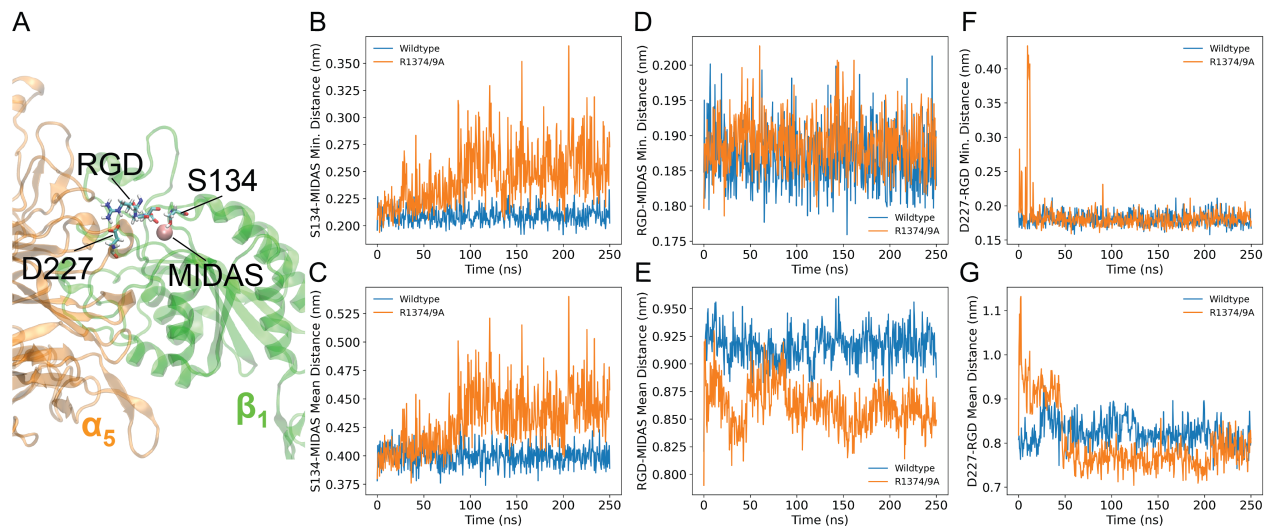


Figure S10: A) RGD site including key molecules such as RGD, S134, and D227, as well as the MIDAS coordination cation. Minimum and mean distances of B-C) S134-MIDAS, D-E) RGD-MIDAS, F-G) D227-RGD.

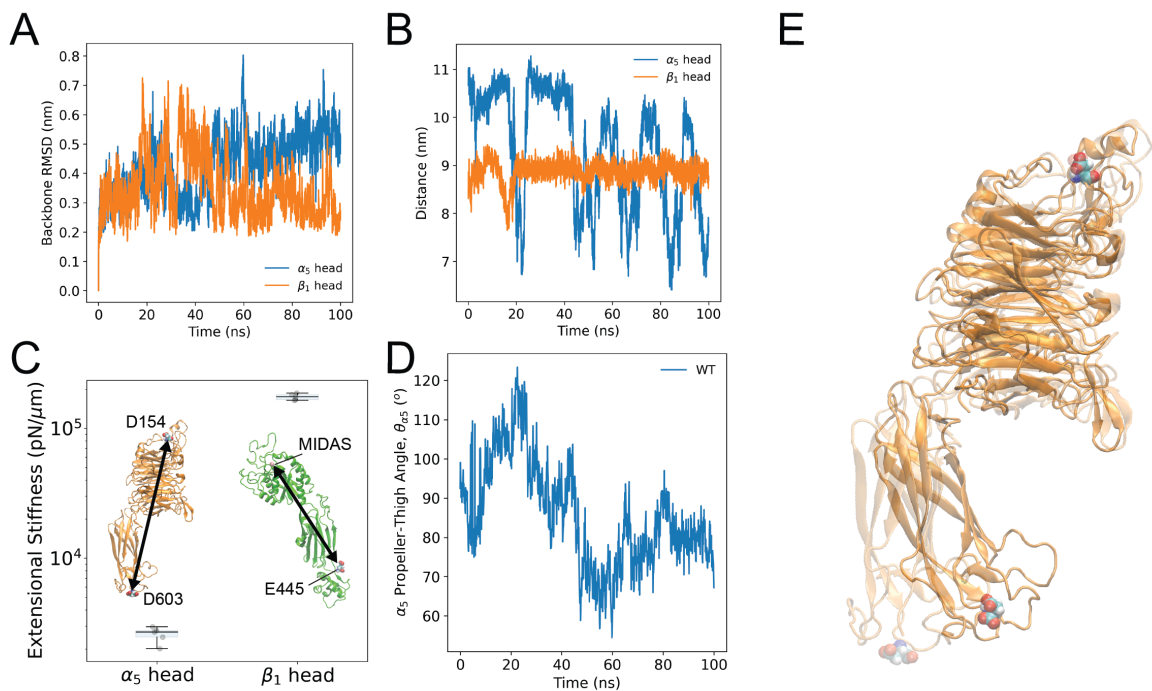


Figure S11: A) Backbone RMSD of independent α_5 and β_1 heads. B) Distance between D603 and D154 (α_5) and E445 and MIDAS (β_1). C) Extensional stiffnesses of α_5 and β_1 as measured by the respective reaction coordinates. D) Propeller-thigh angle on α_5 . E) First (transparent) and last (opaque) frames of α_5 simulation. D603 (top) and D154 (bottom) are shown as references.